The influence of different electrolytes on the electrical and optical properties of polymer films electrochemically synthesized from 3-alkylthiophenes

Thiago Nogueira Marques Cervantes · Danielly Cristina Bento · Elaine Cristina Rodrigues Maia · Ricardo Vignoto Fernandes · Edson Laureto · Gregory J. Moore · Guy Louarn · Henrique de Santana

Abstract In this study, we observed significant differences in the electrical and optical properties of polymer films electrochemically synthesized from two 3-alkylthiophene monomers on platinum wires in 0.100 mol L^{-1} $LiClO_4$/acetonitrile (ACN) or Et_4NBF_4/ACN, when compared to the following homopolymer films: poly(3-methylthiophene) (P3MT), poly(3-hexylthiophene) (P3HT) and poly(3-octylthiophene) (P3OT), prepared under the same conditions. Electrical impedance spectroscopy was used to assess the resistive and capacitive properties of the polymer films [P3MT and P3HT—CP3(MT-HT); P3MT and P3OT—CP3(MT-OT); P3HT and P3OT—CP3(HT-OT)] at overpotentials determined beforehand by Cyclic Voltammetry. The films synthesized in $LiClO_4$/ACN with the lowest charge transfer resistance values were CP3(MT-HT) and CP3(MT-OT), and synthesized in Et_4NBF_4/ACN, CP3(HT-OT). In terms of their optical properties, the films synthesized in $LiClO_4$/ACN exhibited hypsochromic shift of E_g values and a drop in electron affinity values by comparison with homopolymer films and those synthesized in Et_4NBF_4/ACN. Based on Photoluminescence (PL) Spectroscopy it was possible to identify the contributions of the quinone and aromatic segments characteristic of homopolymers in the films synthesized in Et_4NBF_4/ACN. For the films synthesized in $LiClO_4$/ACN, it was not possible to perform the same comparison because there was a discrepancy between the bands observed in the PL images of these materials and those of the homopolymers, suggesting the formation of not only blend structures but also copolymer films. Using Raman Spectroscopy it was possible to identify aromatic, radical cation and dication segments and verify the higher stabilization of radical cation and dication segments in resistive films. It was also possible to observe changes in the morphological structures of the films by comparison with the homopolymers, in addition to alterations due to changes in electrolyte during synthesis using scanning electron microscopy.

1 Introduction

Because of their double conjugate bonds, poly(3-alkylthiophenes) (P3ATs) fall within the group of organic materials of great interest for applications such as battery electrodes, organic light emitting diode (OLED) electronic devices, organic solar cells, low-cost integrated circuits and organic field effect transistors, owing to their good stability, high conductivity and flexibility of preparation [1–7].

After synthesis, these polymers can change from insulators to conductors due to reversible oxidation processes in the π conjugate system, resulting in chains with positive charges, radical cations and dications, which are balanced by the incorporation of counterions (anions), referred to as *p-type* doping [8]. Films obtained in this way exhibit properties that make them efficient electron donors at

T. N. M. Cervantes · D. C. Bento · E. C. R. Maia · H. de Santana (✉)
Departamento de Química, CCE, Universidade Estadual de Londrina, Londrina, PR 86051-990, Brazil
e-mail: hensan@uel.br

R. V. Fernandes · E. Laureto
Depto. de Física, Universidade Estadual de Londrina, Londrina, PR 86051-990, Brazil

G. J. Moore
Yardney Technical Products, Inc., East Greenwich, RI, USA

G. Louarn
Institut des Matériaux Jean Rouxel, Université de Nantes-CNRS, 44322 Nantes, France

heterojunctions with *n-type* materials used in organic solar cells [9].

Adding dopant to the polymer chains produced by the electrolytes results in a dramatic change in the electronic, electrical, magnetic and optical properties of the material, and this process is important for controlling P3ATs [10, 11]. In addition to the redox process resulting from ion activity at the polymer/solution interface, the phenomenon of diffusion in conductive polymers is also associated with other properties of these materials, such as conductivity, morphology, reversibility, permeability, ion selectivity and response time [12].

For this reason, studies have also focused on the type of counterion, i.e. the effect of altered permeability and ion selectivity on charge transport efficiency. Ding et al. [13] report that doping is highly dependent on the nature of the support electrolyte (LiClO₄ and TBAPF₆), associating charge transport inside the polymer with the mobility, input and output of dopant counterions. Borole et al. [14] studied the effect of different inorganic and organic acid electrolytes on the electrochemical properties of electrodes modified by different polymer conductors, such as polyaniline (PANI), poly-orthotoluidine (POT) and PANI–POT copolymer. Using cyclic voltammetry, these authors observed that both current density and conductivity in the polymer phase are strongly influenced by the nature of the anion.

In addition to the influence type of electrolyte on the electrical and optical properties of polymer films, a number of authors [15–24] point out the importance of obtaining new materials by combining the monomer units of two different homopolymers. In earlier studies, electrochemical synthesis of P3ATs and PDFA resulted in materials with lower gap energy values than their respective homopolymers, in addition to variations in electron affinity (*E.A.*) and ionization potential (*I_P*), with the possible application of these copolymers at the electrode/polymer interface of various optoelectronic devices [1]. Feng et al. [25] used the synthesis of P3OT units and units of poly(3-isooctylthiophene) (P3IOT), combining their different photoelectrical properties with the aim of intensifying the luminescence of the new material for applications in OLEDs and organic solar cells.

In our study, we used Electrochemical Impedance Spectroscopy (EIS) as a tool for studying the electrical properties of CP3(MT-HT), CP3(MT-OT) and CP3(HT-OT) polymer films and comparing them with their homopolymer films, synthesized in different electrolytes. Based on results obtained by cyclic voltammetry and UV–Vis spectrophotometry, we also obtained figures for ionization potential, electronic affinity and gap energy (*E_g*), verifying alterations in the properties of homopolymers according to the electrolytes used.

Using photoluminescence (PL) and Raman spectroscopy, it made possible discussion of the influence of

aromatic, radical cation and dication segments, stabilized in polymer films as opposed to homopolymers. This was done to interpret the electrical and optical behaviors observed. The different morphologies were compared with the active areas of the polymer film using scanning electron microscopy (SEM).

2 Experimental section

2.1 Chemicals

The 3-methylthiophene (C_5H_7S), 3-hexylthiophene ($C_{10}H_{16}S$) and 3-octylthiophene ($C_{12}H_{20}S$) monomers were used as received. For support electrolytes, as the salts we used 99 % pure lithium perchlorate ($LiClO_4$) or tetraethylammonium tetrafluoroborate (Et_4NBF_4) supplied by Acros Organics. The solvent was HPLC grade acetonitrile (CH_3CN) with a purity of 99.5 % was obtained from JT Baker.

2.2 Synthesis by chronoamperommetry (CA) and examination by cyclic voltammetry (CV)

The material was synthesized using a platinum wire electrode with an average area of 0.19 cm². All potentials were determined by reference to Ag/AgCl in a Luggin capillary in a solution of 0.100 mol L^{-1} $LiClO_4$ or Et_4NBF_4 in acetonitrile ($LiClO_4$/ACN or Et_4NBF_4/ACN).

Table 1 gives details of the synthesis of films obtained from mixing a solution of 3MT and 3OT, denoted CP3(MT-OT), 3MT and 3HT, denoted CP3(MT-HT) and 3HT and 3OT, denoted CP3(HT-OT). After producing the films, they were immersed in acetonitrile solvent to remove excess low molecular weight species and electrolyte [4].

The CA and CV curves were obtained on an Autolab PGSTAT 302 N potentiostat/galvanostat coupled to a microcomputer running NOVA 1.8.

2.3 Electrochemical impedance spectroscopy (EIS)

The impedance diagrams were obtained on an Autolab PGSTAT 302 N potentiostat with FRAM32 impedance module, varying the frequency from 100 kHz to 0.01 Hz.

2.4 Scanning electron microscopy (SEM)

For SEM analysis, the films were deposited electrochemically at 18 °C in 0.100 mol L^{-1} $LiClO_4$/ACN or 0.100 mol L^{-1} Et_4NBF_4/ACN over indium-doped tin oxide, following the method used by De Santana et al. [4]. The images were obtained on a PHILIPS model Quanta 200 (FEI) electron microscope at voltage between 25 and

Table 1 Chronoamperometry (CA) experimental conditions for films' synthesis

Electrolyte	Films	Concentration (mol L^{-1})			Time (s)	E (V vs. Ag/AgCl)	J (A cm^{-2})
		3MT	3HT	3OT			
LiClO$_4$	P3MT	0.035	–	–	240	1.70	6.05×10^{-6}
	P3HT	–	0.040	–	240	1.75	4.07×10^{-5}
	P3OT	–	–	0.040	240	1.75	8.42×10^{-6}
	CP3(MT-HT)	0.035	0.040	–	240	1.70	2.66×10^{-5}
	CP3(MT-OT)	0.035	–	0.040	240	1.70	1.12×10^{-5}
	CP3(HT-OT)	–	0.040	0.040	240	1.75	4.37×10^{-7}
Et$_4$NBF$_4$	P3MT	0.035	–	–	60	1.60	2.33×10^{-4}
	P3HT	–	0.040	–	240	1.75	6.93×10^{-5}
	P3OT	–	–	0.040	240	1.75	4.26×10^{-5}
	CP3(MT-HT)	0.035	0.040	–	60	1.80	2.86×10^{-4}
	CP3(MT-OT)	0.035	–	0.040	30	1.70	9.68×10^{-5}
	CP3(HT-OT)	–	0.040	0.040	60	1.80	6.67×10^{-5}

Table 2 Anodic potential (E_{ox}), potential variation range (ΔE) and overpotential (η) values for each system determined by films' CVs

Electrolyte	Films	E_{ox} (V vs. Ag$_{(s)}$/AgCl$_{(s)}$)	ΔE (V vs. Ag$_{(s)}$/AgCl$_{(s)}$)	η (V vs. Ag$_{(s)}$/AgCl$_{(s)}$)
LiClO$_4$	P3MT[a]	0.34	0.27:0.65: 0.95: 1.17: 1.35	0.65 ± 0.10
	P3HT	0.65	0.57: 0.66: 0.75: 0.95: 1.10	0.75 ± 0.10
	P3OT[a]	0.72	0.31: 0.84: 1.02: 1.40: 1.58	0.84 ± 0.10
	CP3(MT-HT)	0.36	0.40: 0.46: 0.53: 0.63:0.70	0.70 ± 0.10
	CP3(MT-OT)	0.27	0.40: 0.46: 0.53: 0.63	0.53 ± 0.10
	CP3(HT-OT)	0.53	0.36: 0.56: 0.68: 0.78;0,82	0.82 ± 0.10
Et$_4$NBF$_4$	P3MT	0.38	0.50:0.60:0.70:0.75:0.80	0.50 ± 0.10
	P3HT	0.85	1.00:1.04:1.14:1.35	1.14 ± 0.10
	P3OT	0.91	0.90:1.00:1.05:1.15:1.20:1.25	1.20 ± 0.10
	CP3(MT-HT)	0.76	0.76:0.78:0.79:0.80:0.82:0.85	0.79 ± 0.10
	CP3(MT-OT)	1.11	0.75:0.80:0.90:0.95:1.00:1.50	1.50 ± 0.10
	CP3(HT-OT)	0.86	0.85:0.90:0.92:0.95:1.00:1.05	0.85 ± 0.10

[a] data obtained from (de SANTANA et al. 2013)

30 kV, detector-sample distance from 7.5 to 10.7 mm, and image scale of 10.0–20.0 μm with magnifications of 6000×.

2.5 Spectroscopic characterization

Raman spectra were obtained using a DeltaNu Advantage532® portable Raman spectrometer, excited at 532 nm with resolution of 8 cm^{-1}. NuSpec software (DeltaNu) was used, with baseline resources to remove background fluorescence.

UV–Vis reflectance spectra were obtained using a UV–Vis 2600 spectrophotometer (Shimadzu) coupled to an ISR-2600 integrating sphere. The light source consisted of two lamps: tungsten and deuterium. The spectra were obtained in the 220–900 nm range.

For the photoluminescence experiments we used a 15 mW Ar$^+$ laser excitation source with 405 nm emission line (LASER LINE, FDA, Laser Power supply) recorded on a 0.5 m monochromator, GaAs photomultiplier and synchronous amplifier (lock-in), model RS510 (Stanford). The detection system used was an Ocean Optics USB4000 mini-spectrometer.

3 Results and discussion

Table 2 gives the anodic potential values (E_{ox}), potential variation range (ΔE) and overpotentials (η) of each system (based on voltammograms) used in the Electrochemical Impedance Spectroscopy (EIS). The cyclic voltammograms of the films deposited on the platinum wire
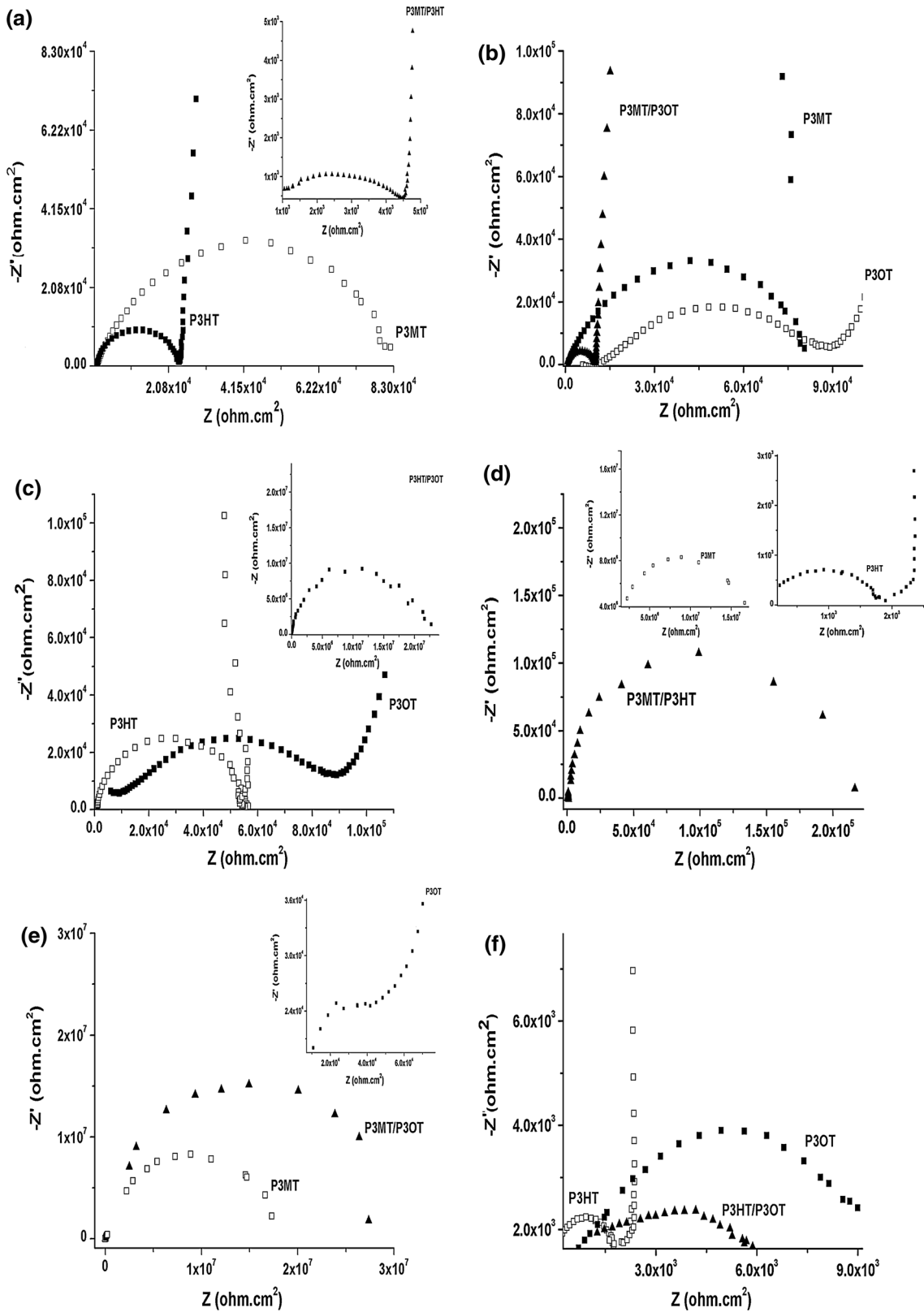
◀ **Fig. 1** Nyquist plots obtained at an overpotential for the films deposited on a platinum plate in 0.100 mol L^{-1} LiClO$_4$/ACN:**a** (*white square*) P3HT, (*black square*) P3MT and (*black down-pointing triangle*) CP3(MT-P3HT). **b** (*white square*) P3MT, (*black square*) P3OT and (*black down-pointing triangle*) CP3(MT-OT); **c** (*white square*) P3HT, (*black square*) P3OT and (*black down-pointing triangle*) CP3(HT-OT). And deposited on a platinum plate in 0.100 mol L^{-1} Et$_4$NBF$_4$/ACN: **d** (*white square*) P3MT, (*black square*) P3HT and (*black down-pointing triangle*) CP3(MT-HT). **e** (*white square*) P3MT, (*black square*) P3OT and (*black down-pointing triangle*) CP3(MT-OT); **f** (*white square*) P3HT, (*black square*) P3OT and (*black down-pointing triangle*) CP3(HT-OT)

duplicated the results obtained from films produced on platinum plates of greater surface area [1, 4].

Figure 1 shows the Nyquist plots, −Z″ versus Z′ curves, of the films produced over platinum in 0.100 mol L^{-1} LiClO$_4$/ACN and in 0.100 mol L^{-1} Et$_4$NBF$_4$/ACN obtained at overpotential. Some diagrams are highlighted to clarify the curves.

In the diagrams in Fig. 1, we expected to see two high-frequency semicircles induced by the charge transport processes at the metal/polymer and polymer/solution interfaces. However, similar to studies on these P3ATs with polydiphenylamine (PDFA) [26], we observed only one semicircle. This was probably due to the homogeneous non-separation of the surfaces, partial superpositions of these semicircles or the characteristics of the interface processes in terms of resistance at the polymer/solution interface [27]. The decisive stage in this last process is ion transport [28]. Since the materials studied are *p-type* polymers [29] and they were polymerized by anodic oxidation, this decisive stage involves the incorporation of anions (ClO$_4^-$ or BF$_4^-$) in the pores of the material, whose matrix is positively charged by *polarons* (radical cations)/*bipolarons* (radical dications) that are stabilized precisely by these counterions acting as dopants [30].

These ions are basically in two states: adsorbed or trapped in the polymer matrix, and the trapped ions are expelled from the material only when very negative potentials are applied [13]. Therefore, under the electrochemical impedance experimental conditions, the effect observed at high frequencies was merely the incorporation of (adsorbed or trapped) anions in the polymer matrix. Thus, the extension of the diameters of the semicircle in the Nyquist plots is related to the accumulation of ClO$_4^-$ or BF$_4^-$ anions in the polymer matrix.

Another relevant observation at high frequencies was the altered shape of the semicircle produced by changing the electrolyte from LiClO$_4$/ACN to Et$_4$NBF$_4$/ACN. This was probably due to the lower homogeneity in the thickness and concentration of the film synthesized in Et$_4$NBF$_4$/ACN, resulting in a concentration of material in distinct areas, impeding charge transport [31].

Table 3 Charge transfer resistance (R$_{CT}$) of the films obtained from Nyquist plots at an overpotential

Films	Electrolyte	
	LiClO$_4$/ACN R$_{CT}$ (ohm cm^2)	Et$_4$NBF$_4$/ACN
P3MT	7.81×10^{4a}	1.47×10^7
P3HT	5.38×10^4	1.67×10^3
P3OT	7.91×10^{4a}	3.09×10^4
CP3(MT-HT)	3.52×10^3	2.16×10^5
CP3(MT-OT)	9.43×10^3	2.64×10^7
CP3(HT-OT)	2.28×10^7	5.01×10^3

[a] data obtained from (de SANTANA et al. 2013)

Table 4 Gap energy (E$_g$), ionization potential (I$_p$), and electron affinity (E.A) parameters of films electrochemically synthesized at the presence of LiClO$_4$/ACN or Et$_4$NBF$_4$/ACN as electrolyte

Electrolyte	films	λ_{max} (nm)	E'_{OX} (V)	I_p (eV)	E_g (eV)	E.A. (eV)
LiClO$_4$	P3MT[a]	451	0.34	4.7	2.7	2.0
	P3HT[a]	447	0.65	5.0	2.8	2.3
	P3OT[a]	432	0.72	5.1	2.9	2.2
	CP3(MT-HT)	396	0.36	4.8	3.1	1.6
	CP3(MT-OT)	400	0.27	4.7	3.1	1.6
	CP3(HT-OT)	380	0.53	4.9	3.3	1.7
Et$_4$NBF$_4$	P3MT[a]	449	0.38	4.8	2.8	2.0
	P3HT	438	0.85	5.2	2.8	2.4
	P3OT[a]	441	0.91	5.3	2.8	2.5
	CP3(MT-HT)	433	0.76	5.2	2.9	2.3
	CP3(MT-OT)	440	1.11	5.5	2.8	2.7
	CP3(HT-OT)	440	0.86	5.3	2.8	2.4

Obs E$_g$, I$_p$ and E.A. were defined by λ_{max}, E'_{OX} and subtracting the I$_p$ from E$_g$, respectively. [a]data obtained from [CERVANTES et al., 2012; de SANTANA et al., 2013]

Furthermore, at medium frequencies we observed straight segments angled at 45° corresponding to the Warburg impedance, reflecting the semi-infinite diffusion-migration of ions under boundary conditions (between polymer and solution). At low frequencies, we observed straight segments tending to be angled at 90°, characteristic of the capacitive impedance due to charge transport within the bulk of the solution [28]. In some cases, such as CP3(HT-OT) and CP3(MT-OT)/CP3(MT-HT) synthesized respectively in LiClO$_4$/ACN and in Et$_4$NBF$_4$/ACN, we observed shifts in the Warburg impedance to low frequency regions. This was due to the low ionic conductivity under boundary conditions, resulting from a thin diffusion layer in the polymer [28]. In these situations, capacitive impedance cannot be observed.

Fig. 2 PL spectra of CP3(MT-HT), CP3(MT-OT) and CP3(HT-OT) synthesized in **a** LiClO$_4$/ACN e **b** Et$_4$NBF$_4$/ACN. *Asterisk* at Fig. 2b, the CP3(MT-OT) spectrum "saturated the signal" when a 2s integration time was utilized. Thus, the spectrum was obtained at integration time of 10^{-1} s
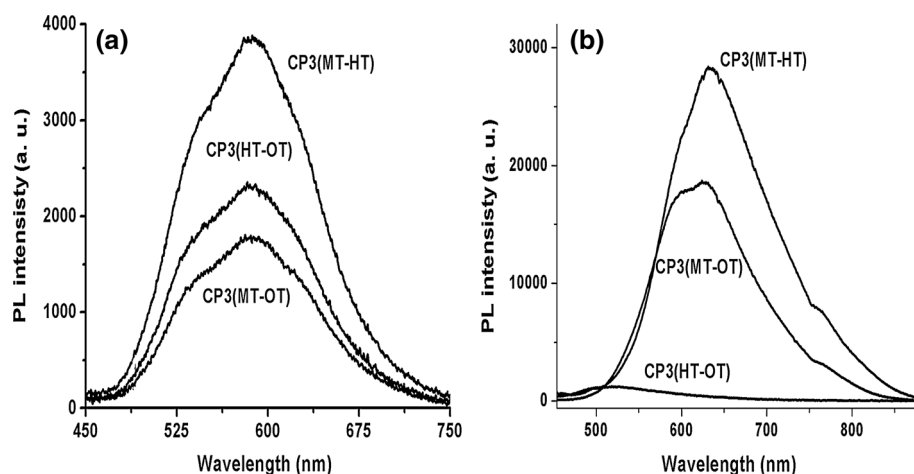
Based on the diagrams in Fig. 1, it was possible to calculate R$_{CT}$ values for the films by subtracting the final semicircle resistance from the initial semicircle resistance. The results are given in Table 3.

The data in Table 3 also show that changing the electrolyte from LiClO$_4$/ACN to Et$_4$NBF$_4$/ACN significantly changes the R$_{CT}$ values, both for homopolymers and the materials obtained from mixing their monomers. When the films were produced in LiClO$_4$/ACN, R$_{CT}$ values increased in the following sequence: CP3(MT-HT) < CP3(MT-OT) < P3HT < P3MT < P3OT < CP3(HT-OT). For films produced in Et$_4$NBF$_4$/ACN, these values increased in the following sequence: P3HT < CP3(HT-OT) < P3OT < CP3(MT-HT) < P3MT < CP3(MT-OT). Based on these data, note that CP3(MT-HT) exhibited the lowest R$_{CT}$ value when synthesized in LiClO$_4$/ACN (3.52 × 10^3 ohm cm^2), and when synthesized in Et$_4$NBF$_4$/ACN, it was one of the polymers exhibiting the highest R$_{CT}$ value (2.16x10^5 - ohm cm^2), representing an increase of approximately 60 times. In contrast, CP3(HT-OT), when synthesized in LiClO$_4$/ACN, exhibited the highest R$_{CT}$ value (2.28 × 10^7 - ohm cm^2), but in Et$_4$NBF$_4$/ACN the R$_{CT}$ value was 4,550 times lower (5.01 × 10^3 ohm cm^2).

These differences in R$_{CT}$ values are closely linked to the accumulation of counterions (ClO$_4^-$ or BF$_4^-$) in the polymer matrix at the different overpotentials applied [28]. In CP3(MT-OT) and CP3(MT-HT) films, the ClO$_4^-$ ion diffusion-migration process is more efficient than that of the BF$_4^-$ anion. In contrast, the reverse was the case for CP3(HT-OT). This phenomenon is probably due to a greater interaction of ClO$_4^-$ ions with the polymer matrices of CP3(MT-OT) and CP3(MT-HT), and BF$_4^-$ ions in CP3(HT-OT). The higher doping level in these cases could be related to the stabilization of these counterions due to coulombic attraction between the counterions and positively-charged radical cation and dication segments present in greater quantities in the matrices of the films mentioned [2].

Table 4 gives the values of the following optical properties: E$_g$, I$_p$ and E.A., as a function of the electrolyte used for synthesizing the films produced by mixing the 3-alkylthiophenes, with the aim of comparing the results obtained for the P3MT, P3HT and P3OT polymers.

Based on the values in Table 4, we concluded that the films of CP3(MT-HT), CP3(MT-OT) and CP3(HT-OT) synthesized in LiClO$_4$/ACN showed a drop in the values of E.A. and a shift of E$_g$ values toward the blue end of the spectrum for both the homopolymers prepared in this electrolyte and for the films synthesized in Et$_4$NBF$_4$/ACN. According to Perepichka et al. [32], this effect could be related to the presence of a preferential coupling between thiophene rings, i.e. in the same position relative to the side chain. Polymerization causes torsion between the units of 3-alkylthiophenes in the extension of the polymer chain, with the concomitant loss of conjugation. The presence of coupling in irregular poly(3-alkylthiophenes) is expected to cause increased torsion of the thiophene ring units, due to steric repulsion. This in turn increases the gap energy and causes other spurious changes in electronic properties. Since the hypsochromic shift was more significant for the CP3(HT-OT), this suggests that the increased torsion in this material is due to the nature of the alkyl side chains involved. In this process of film formation, the electrolyte significantly influences the electronic properties of the material.

Figure 2 shows the PL spectra of the films of CP3(MT-HT), CP3(MT-OT) and CP3(HT-OT) synthesized in (a) LiClO$_4$/ACN and (b) Et$_4$NBF$_4$/ACN, for assessing the emission from their constituent species synthesized in different electrolytes.

The PL spectra in Fig. 2b show that the films of CP3(MT-OT) and CP3(MT-HT) synthesized in Et$_4$NBF$_4$/ACN exhibit an emission intensity higher than that of the other films produced by mixing the 3-alkylthiophenes. This was predictable since these materials are more resistive than the other films [33].

Fig. 3 PL spectra deconvoluted of polymeric films: CP3(MT-HT) in **a** LiClO$_4$/ACN and **a'** Et$_4$NBF$_4$/ACN; CP3(MT-OT) in **b** LiClO$_4$/ACN and **b'** Et$_4$NBF$_4$/ACN; CP3(HT-OT) in **c** LiClO$_4$/ACN and **c'** Et$_4$NBF$_4$/ACN
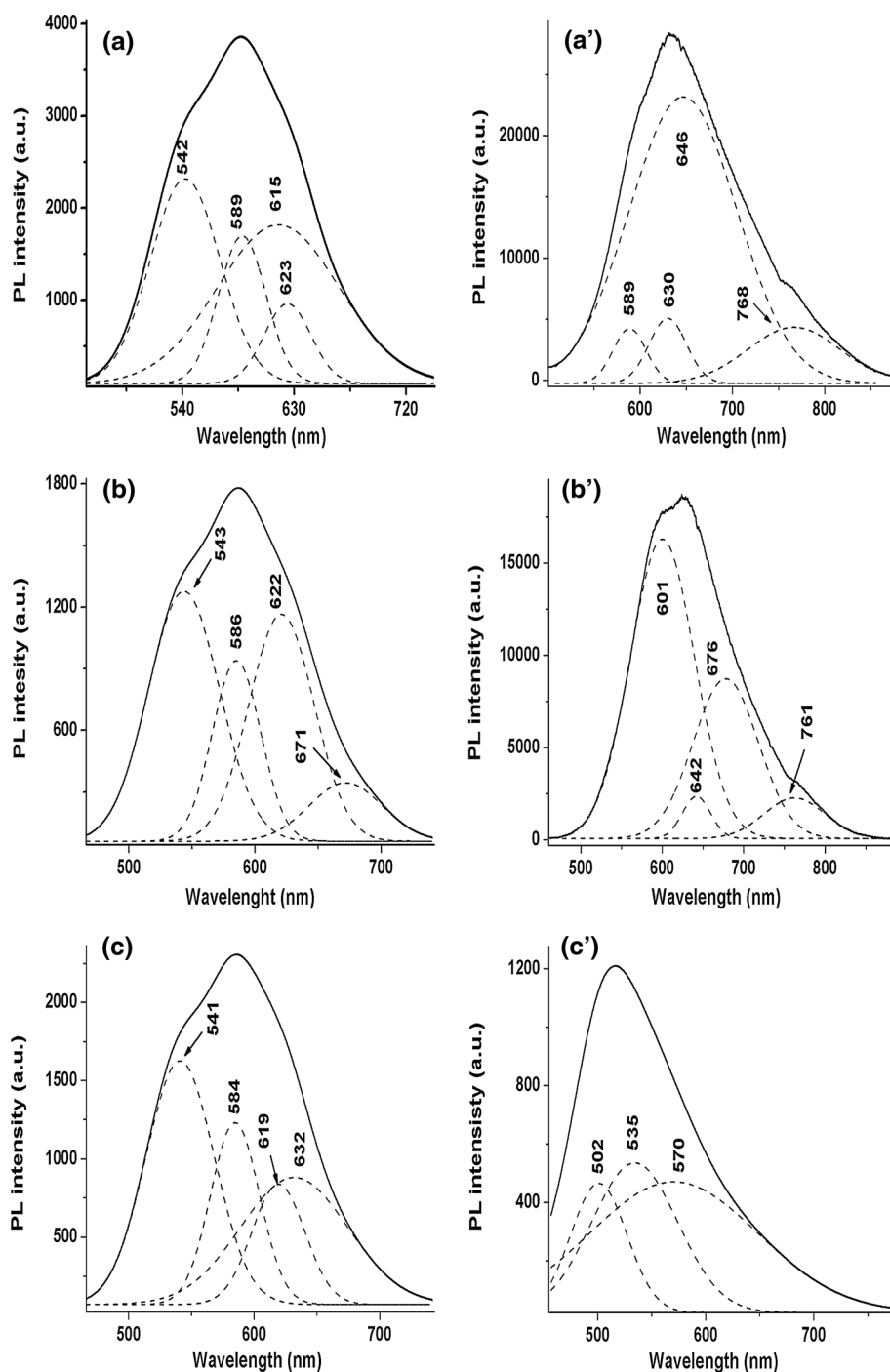
The exception was the low emission of CP3(HT-OT) synthesized in LiClO$_4$/ACN (Fig. 2a). Since its resistivity is similar to that of CP3(MT-OT) synthesized in Et$_4$NBF$_4$/ACN (Table 3), an intense PL signal is to be expected for this material. As mentioned above, this behavior is also associated with increased torsion in the polymer chain of this material [32].

Figure 3 shows the deconvoluted PL spectra of copolymers CP3(MT-HT), CP3(MT-OT) and CP3(HT-OT)

synthesized in LiClO$_4$/ACN and Et$_4$NBF$_4$/ACN, in the regions between 450 and 750 nm (LiClO$_4$/ACN) and between 450 and 900 nm (Et$_4$NBF$_4$/ACN). This procedure was used in order to characterize the contributions of quinonic and aromatic segments to the emission behavior of the materials [34].

In all the deconvoluted PL spectra of CP3(MT-HT), CP3(MT-OT) and CP3(HT-OT) synthesized in LiClO$_4$/ACN (Fig. 3 a, b, c) we verified four contributions with
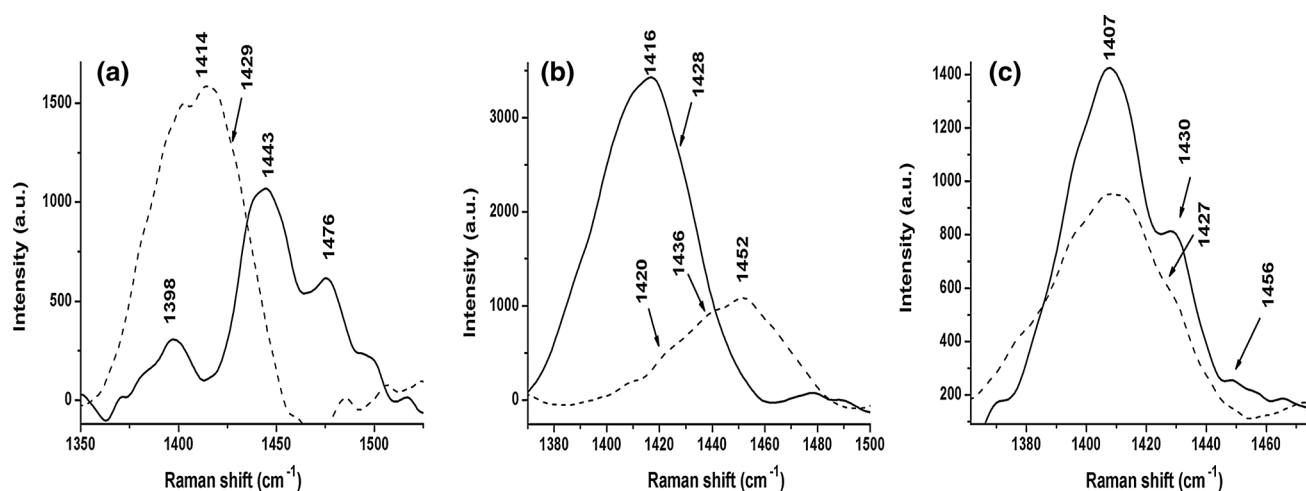
Fig. 4 Raman spectra of materials as deposited on a platinum wire in 0.100 mol L^{-1} LiClO$_4$/ACN (*endash*) and (*emdash*) Et$_4$NBF$_4$/ACN. **a** CP3(MT-HT); **b** CP3(MT-OT) and **c** CP3(HT-OT). λ = 532 nm

close relative intensities. These exhibited significant shifts in relation to the two contributions (quinonic and aromatic) observed in homopolymers synthesized in LiClO$_4$/ACN, at 505/576, 486/533, 514/574 for P3MT, P3HT and P3OT, respectively [35, 36]. These variations in the observed contributions by comparison with the contributions in the homopolymers confirm that there is no blend formation, but that the material synthesized electrochemically exhibits strong interactions between the chains, probably producing copolymer chains.

In Fig. 3(a′, b′), the deconvoluted PL spectra of the films synthesized in Et$_4$NBF$_4$/ACN show four contributions with fairly different relative intensities. They do not show marked shifts in emission maxima compared with the contributions of the homopolymers and therefore it was possible to detail the contributions of the quinonic/aromatic segments of the homopolymers in these materials. In the PL spectra of homopolymers synthesized in Et$_4$NBF$_4$/ ACN, we observed bands centered on 639/754, 580/626, 510/565 for P3MT, P3HT and P3OT respectively.

In the PL spectrum in Fig. 3(a′), the intense contributions at 646 and 768 nm relate to the quinonic/aromatic segments of P3MT [34, 37], in greater quantity in the material, whereas the low intensities at 589 and 630 nm relate to the segments of P3HT [36], present in lower quantity. For the PL spectrum in Fig. 3(b′), the characteristic bands of the quinonic/aromatic forms of P3OT exhibited in this material appear intense and shifted to 601 and 676 nm. The other bands at 642 and 761 nm relate to the lower contributions of the units of P3MT.

In Fig. 3(c′) we observed only three contributions in the deconvoluted PL spectrum. Those at 502 and 535 nm were similar to those observed in the PL spectrum of the P3OT homopolymer and attributed to the quinonic and aromatic

segments [34, 37]. The wide band observed at 570 nm can be treated as relating to the quinonic form of P3HT.

Therefore, the electrochemical synthesis of the films in Et$_4$NBF$_4$/ACN probably consisted merely of the formation of blends.

Figure 4 shows the Raman spectra of the films synthesized in 0.100 mol L^{-1} LiClO$_4$/ACN or 0.100 mol L^{-1} Et$_4$NBF$_4$/ACN, with the aim of detailing the characterization of species present in the matrices of the material synthesized in different electrolytes.

The spectra relate to the region of frequencies characteristic of symmetric C=C stretching of the thiophene ring, since this vibrational mode was sensitive to the modifications undergone in the thiophene ring of the homopolymers [1, 4, 35, 36]. Despite the interval analyzed, the band at 1,398 cm^{-1} was discarded since it was ascribed to symmetric C–C stretching of the ring [4]. After expanding the spectra, we checked for the presence of shoulders in the spectra of the materials as prepared, highlighted in Fig. 4.

The spectrum of CP3(MT-HT) synthesized in LiClO$_4$/ ACN (Fig. 4a) shows the frequencies at 1,476 and 1,443 cm^{-1}. The last value shifts to 1,414 cm^{-1} in the spectrum of the material synthesized in Et$_4$NBF$_4$/ACN. In the spectra of CP3(MT-OT) (Fig. 4b), there is a shift from the band at 1,416 cm^{-1} (synthesis in LiClO$_4$/ACN) toward 1,452 cm^{-1} (synthesis in Et$_4$NBF$_4$/ACN). In Fig. 4c, the band centered on 1,407 cm^{-1} in the spectra of CP3(HT-OT) is merely intensified and widened, although in the spectrum of the film synthesized in LiClO$_4$/ACN, shoulders at 1,430 and 1,456 cm^{-1} are also visible.

Table 5 gives the characteristic frequencies of the aromatic, dication and radical cation segments of the thiophene ring in the region between 1,400 and 1,500 cm^{-1}, found in the Raman spectra of the polymer and

Table 5 Relation of characteristic Raman frequencies of the homopolymers in different electrolytes and their correlation with those obtained in the polymeric films

Segments	Raman frequencies (cm^{-1})											
	[b]P3MT		[b]P3HT		[b]P3OT		CP3(MT-HT)		CP3(MT-OT)		CP3(HT-OT)	
	LiClO$_4$	Et$_4$NBF$_4$	LiClO$_4$	Et$_4$NBF$_4$	LiClO$_4$	Et$_4$NBF$_4$	LiClO$_4$	Et$_4$NBF$_4$	LiClO$_4$	Et$_4$NBF$_4$	LiClO$_4$	Et$_4$NBF$_4$
Aromatic	1,431	1,406	1,442	1,426	1,443	1,404	–	1,414	1,416	1,420[a]	1,407	1,407
Dication	1,437	1,431	1,470	1,451	1,465	1,430	1,443	1,429[a]	1,428[a]	1,436[a]	1,430	1,427[a]
Radical Cation	1,470	1,476	1,492	1,465	1,498	1,461	1,476	–	–	1,452	1,456[a]	–

[a] shoulder; [b] data obtained from (Cervantes et al. 2012; de Santana et al. 2013)

homopolymer films. The homopolymer frequencies were obtained from previous studies [4, 35, 36].

The frequencies in Table 5 show the simultaneous presence of aromatic and dication segments in the matrices of the CP3(MT-OT) and CP3(HT-OT) films synthesized in both electrolytes. In the CP3(MT-HT) matrix, the simultaneous occurrence of these two segments was observed only when the material was synthesized in Et$_4$NBF$_4$/ACN; the aromatic segment is absent from the film synthesized in LiClO$_4$/ACN. However, the radical cation species was observed in the matrices of the CP3(MT-HT) and CP3(HT-OT) films synthesized in LiClO$_4$/ACN and in the CP3(MT-OT) film synthesized in Et$_4$NBF$_4$/ACN.

According to the resistance figures in Table 3, CP3(MT-HT) was the least resistive and CP3(MT-OT) and CP3(HT-OT) the most resistive of the films synthesized in LiClO$_4$/ACN. Based on the results of Raman spectroscopy, this behavior of CP3(MT-HT) could be related to the stabilization of the radical cation and dication segments in the matrix of this copolymer, boosting the diffusion-migration process of the ClO$_4^-$ dopant because of the greater interaction between the positively charged segments and this counterion, contributing to increased conductivity along the chains of these copolymers. The higher resistivity of the CP3(MT-OT) and CP3(HT-OT) films could be related to the low accumulation of ClO$_4^-$ caused by the presence of the aromatic segment in the matrices of these materials.

Of the materials synthesized in Et$_4$NBF$_4$/ACN, CP3(HT-OT) exhibited the lowest resistivity (Table 3). Based on the data in Table 5, we can see that the segments include the simultaneous presence of the aromatic and dication species. The higher conductivity of this material could therefore be related to the accumulation of the dopant ion BF$_4^-$, possibly stabilized by coulombic attraction to the dication segment in the matrix of this material.

Based on the Raman spectra, the discrepancy in the frequencies obtained becomes pronounced when BF$_4^-$ is used at the dopant instead of ClO$_4^-$. The shifts observed and the variation in their intensities back up the

conclusions on the changes in the R$_{CT}$ values (Table 3), where the increased presence of radical cation and dication species could be related to lower resistivity, due to the greater coulombic interaction between these species and the dopant.

Figure 5 shows the micrographs of the P3MT, P3HT and P3OT polymers and the films of CP3(MT-HT), CP3(MT-OT) and CP3(HT-OT) synthesized in solutions of 0.100 mol L^{-1} LiClO$_4$/ACN and Et$_4$NBF$_4$/ACN. The images show the cauliflower and *packed grain* structures characteristic of conductive polymers [38, 39], highlighting the morphological differences between the homopolymers and polymer films [40], and between the materials synthesized in different electrolytes.

The images of the P3HT and P3OT films doped with BF$_4^-$, and those of the P3MT, CP3(MT-HT) and CP3(MT-OT) films doped with ClO$_4^-$ characterize the three-dimensional growth of the polymers as aggregates uniformly distributed over the surface of the electrode. This kind of morphology could increase the active area of the materials and favor charge transfer along the material, and this could be why these films show less resistive behavior as shown in the Nyquist plots (Fig. 1a, b) [1, 41].

The images of the P3HT and P3OT doped with ClO$_4^-$ and the P3MT, CP3(MT-HT) and CP3(MT-OT) films doped with BF$_4^-$, characterize the three-dimensional growth of the polymers as packed grain structures, consisting of areas of high material concentration containing empty spaces, resulting in heterogeneous surfaces of lower active area [38]. These films showed resistive behavior, assumedly due to this characteristic impeding charge transport.

The CP3(HT-OT) film doped with ClO$_4^-$ showed three-dimensional polymer growth with aggregates uniformly distributed over the electrode surface, whereas the same copolymer film doped with BF$_4^-$ showed three-dimensional growth with packed grain structures, consisting of areas of high material concentration containing empty spaces. Due to this morphological difference, the CP3(HT-OT) doped
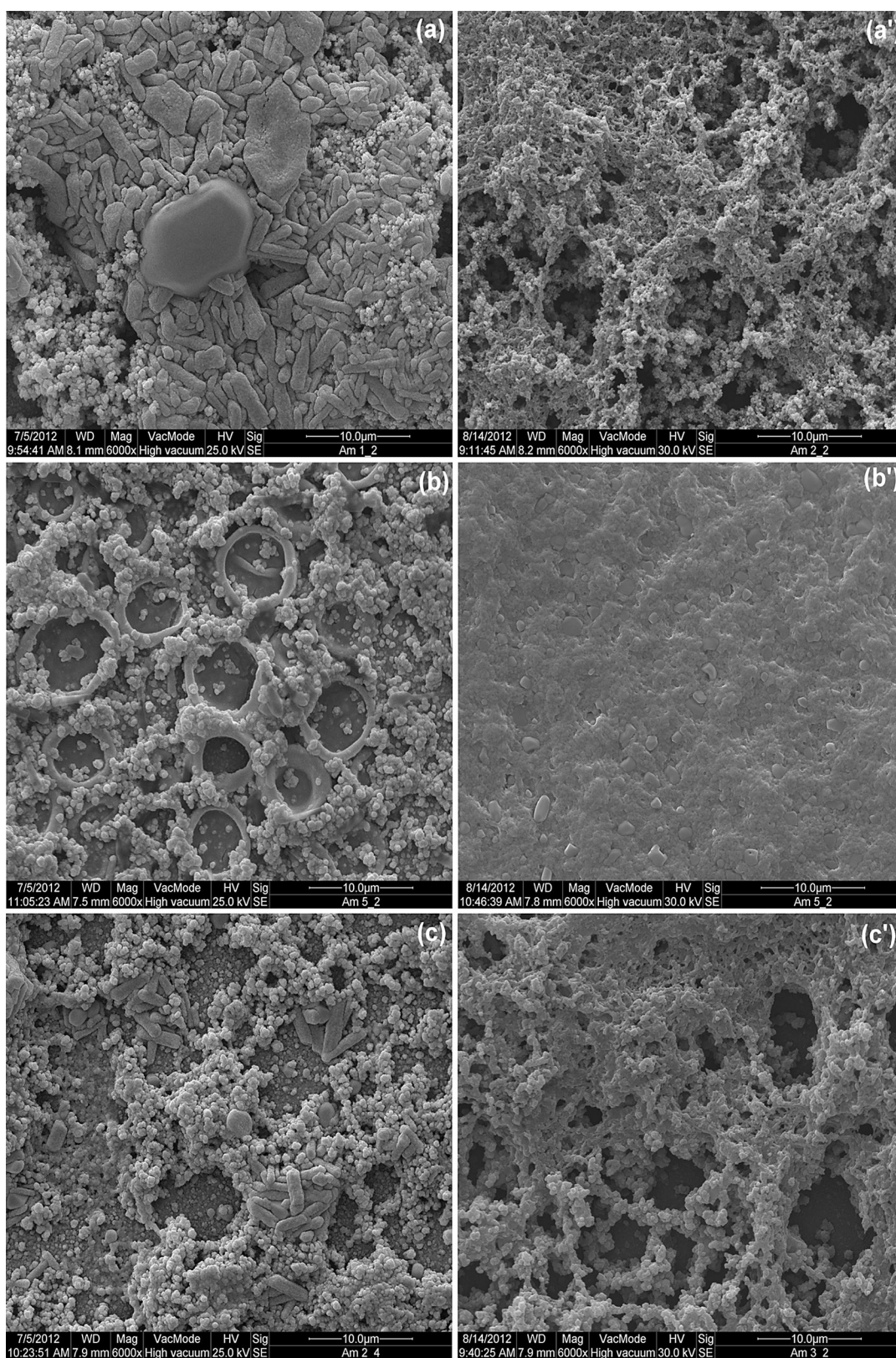
Fig. 5 Micrographs of homopolymers and polymeric films synthesized in LiClO$_4$/ACN **a** P3MT, **b** P3HT, **c** P3OT, **d** CP3(MT-HT), **e** CP3(MT-OT) and **f** CP3(HT-OT); and synthesized in Et$_4$NBF$_4$/ACN **a′** P3MT, **b′** P3HT, **c′** P3OT, **d′** CP3(MT-HT), **e′** CP3(MT-OT) and **f′** CP3(HT-OT)
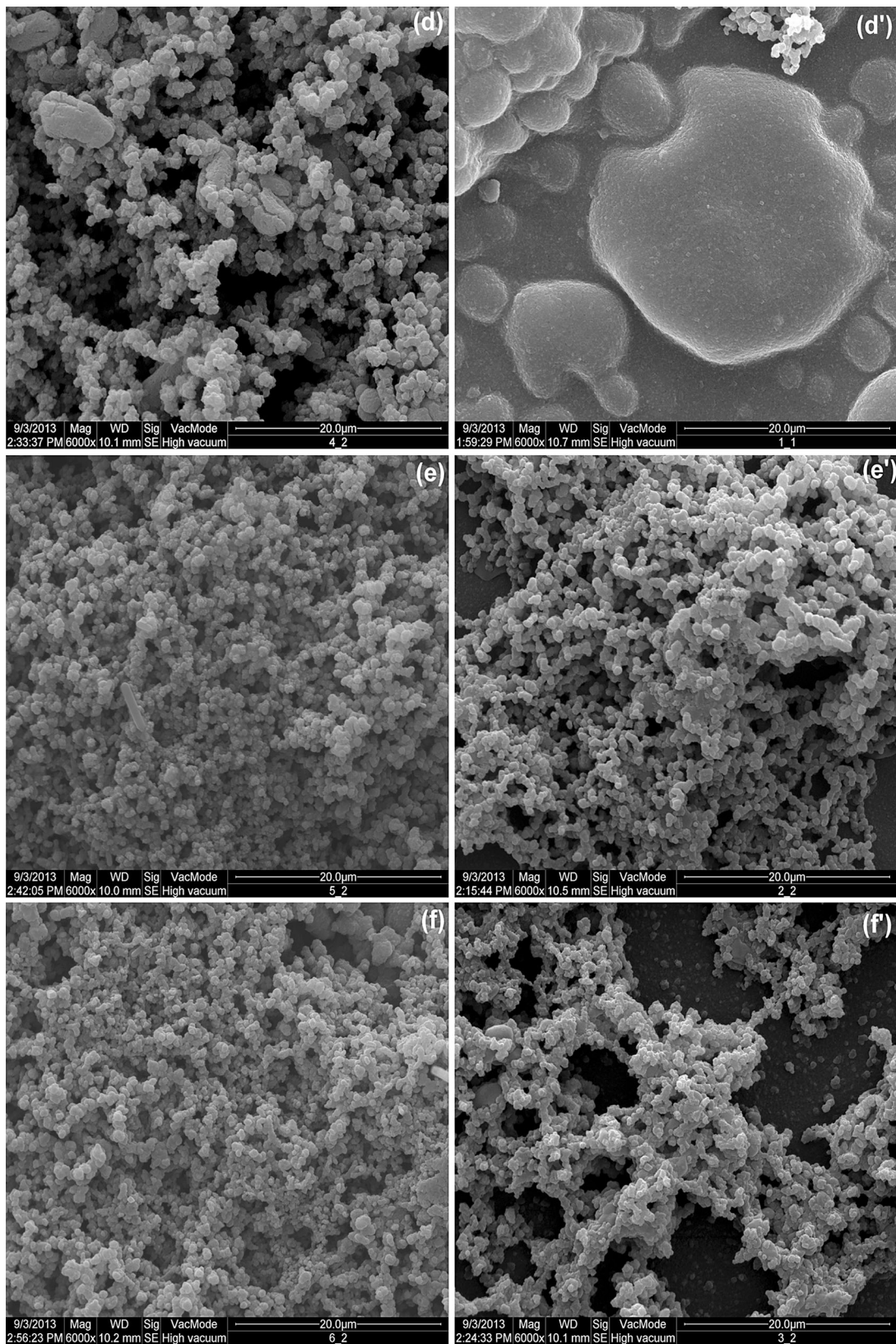
Fig. 5 continued

with ClO_4^- showed a higher active area compared to the material doped with BF_4^-. We would therefore expect the first film to show lower resistive behavior. However, in this case the charge transfer resistance cannot be related only to the morphology of the material, since the film doped with BF_4^- showed a considerable drop in resistivity (Table 3).

4 Conclusion

The results obtained showed that the nature of the electrolyte used for electrochemical synthesis ($LiClO_4$ or Et_4NBF_4) influenced the electrical and optical properties of the polymer films produced. Using EIS it was possible to determine the charge transfer resistance values (R_{CT}) of these films and compare them with homopolymers, all at overpotentials. The CP3(MT-HT) and CP3(HT-OT) films showed lower resistivity when synthesized in $LiClO_4$/ACN, whereas the CP3(HT-OT) film showed lower resistivity when synthesized in Et_4NBF_4/ACN. This difference was due to a higher level of doping cause by the stabilization of ClO_4^- or BF_4^- counterions as a result of coulombic attraction between these ions and the positively charged radical cation and dication species present in higher quantities in the matrix. This conclusion was put to the test using Raman Spectroscopy, which confirmed the stabilization of radical cation and dication segments in materials with lower R_{CT} values.

PL spectroscopy confirmed that the CP3(MT-HT) and CP3(MT-OT) films synthesized in Et_4NBF_4/ACN exhibited an intense PL signal, significantly stronger than the other polymer films. We also observed that the CP3(HT-OT) film synthesized in $LiClO_4$/ACN, from which we expected an intense PL signal, showed low emission. This was probably due to the greater torsion of the polymer chain in films synthesized in this electrolyte. This effect is also related to the shift in E_g values toward the blue end of the spectrum and a drop in $E.A.$ values. By deconvoluting the PL spectra, we were able to infer that there was no blend structure formation in polymers synthesized in $LiClO_4$/ACN, but rather copolymer films.

Finally, SEM allowed us to observe the changes in the morphological structures of polymer films compared to homopolymers, showing the higher active area of polymer films doped with ClO_4^- compared to those doped with BF_4^-. By SEM it was also possible to relate the low-resistivity behavior of most of the polymer films to the morphology of these materials synthesized in $LiClO_4$/ACN.

References

1. D.C. Bento, E.C.R. Maia, T.N.M. Cervantes, R.V. Fernandes, E. Di Mauro, E. Laureto, M.A.T. Da Silva, J.L. Duarte, I.F.L. Dias, H. de Santana, Synth. Met. **162**, 2433 (2012)
2. F.M. Nodari, R.L. Patyk, L.S. Roman, A.R.V. Benvenho, I.A. Hummelgen, E.K.C. Yoshikawa, J. Gruber, J. Mater. Sci.: Mater. Electron. **21**, 1235 (2010)
3. C.H. Kim, K. Kisie, J. Jung, J. Ulansk, D. Tondeliera, B. Geffroya, Y. Bonnassieuxa, G. Horowitza, Synth. Met. **162**, 460 (2012)
4. H. de Santana, E.C.R. Maia, D.C. Bento, T.N.M. Cervantes, G.J. Moore, J. Mater. Sci.: Mater. Electron. **24**, 3352 (2013)
5. R. Singh, J. Kumar, R.K. Singh, A. Kaur, K.N. Sood, R.C. Rastogi, Polymer **46**, 9126 (2005)
6. G. Inzelt, M. Pineri, J.W. Schultze, M.A. Vorotyntsev, Electrochim. Acta **45**, 2403 (2000)
7. E.G. Tolstopyatova, S.N. Sazonova, V.V. Malev, V.V. Kondratiev, Electrochim. Acta **50**, 1565 (2005)
8. J.D. Stenger-Smith, Prog. Polym. Sci. **23**, 57 (1990)
9. C.L. Chochos, S.A. Choulis, Prog. Polym. Sci. **36**, 1326 (2011)
10. A.G. MacDiarmid, Angew. Chem. Int. Ed. **40**, 2581 (2001)
11. W.J. Feast, J. Tsibouklis, K.L. Pouwer, L. Groenendaal, E.W. Meijer, Polymer **37**, 5017 (1996)
12. A. Ray, A.F. Richter, A.G. Macdiarmid, J. Epstein, Synth. Met. **29**, 151 (1989)
13. H. Ding, L. Pigani, R. Seeberb, C. Zanardi, J. New Mater. Electrochem. Syst. **3**, 339 (2000)
14. D.D. Borole, U.R. Kapadi, P.P. Kumbhar, D.G. Hundiwale, Mater. Lett. **57**, 844 (2002)
15. E. Zhou, Z. Tan, Y. He, C. Yang, Y. Li, J. Polym. Sci. A: Polym. Chem. **45**, 629 (2007)
16. Y. Li, L. Xue, H. Xia, B. Xu, S. Wen, W. Tian, J. Polym. Sci. A: Polym. Chem. **46**, 3970 (2008)
17. W. Lee, H. Choi, S. Hwang, J.Y. Kim, H.Y. Woo, Chemistry **18**, 2551 (2012)
18. L.M. Chen, Z.R. Hong, G. Li, Y. Yang, Adv. Mater. **21**, 1434 (2009)
19. Q. Zhang, A. Cirpan, T.P. Russell, T. Emrick, Macromolecules **42**, 1079 (2009)
20. J. Ohshita, Y. Tada, A. Kunai, Y. Harima, Y. Kunugi, Synth. Met. **159**, 214 (2009)
21. Y. He, W. Wu, Y. Liu, Y. Li, J. Polym. Sci. A: Polym. Chem. **47**, 5304 (2009)
22. K. Lu, X. Sun, Y. Liu, C. Di, H. Xi, G. Yu, X. Gao, C. Du, J. Polym. Sci. A: Polym. Chem. **47**, 1381 (2009)
23. D. Izuhara, T.M. Swager, J. Am. Chem. Soc. **131**, 17724 (2009)
24. N. Sary, F. Richard, C. Brochon, N. Leclerc, P. Leveque, J.N. Audinot, T. Heiser, G. Hadziioannou, R. Mezzenga, Adv. Mater. **22**, 763 (2010)
25. W.D. Feng, Z.J. Qi, Y.M. Sun, Eur. Polym. J. **43**, 3638 (2007)
26. D.C. Bento, E.C.R. Maia, P.R.P. Rodrigues, G. Louarn, H. de Santana, J. Mater. Sci.: Mater. Electron. **24**, 4732 (2013)
27. J.R. MacDonald, Electrochim. Acta **35**, 1483 (1990)
28. H. Ding, Z. Pan, L. Pigani, R. Seeber, C. Zanardi, Electrochim. Acta **46**, 2721 (2001)
29. Q. Xue, O. Harriman, M.C. Leake, J. Phys. Conf Ser **286**, 1 (2011)
30. S. Fletcher, J. Chem. Soc. Faraday Trans. **89**, 311 (1993)

31. Y. Li, J. Gao, G. Yu, Y. Cao, A.J. Heeger, Chem. Phys. Lett. **287**, 83 (1998)
32. I.F. Perepichka, D.F. Perepichka, H. Meng, F. Wudl, Adv. Mater. **17**, 2281 (2005)
33. Y.J. Cheng, S.H. Yang, C.S. Hsu, Chem. Rev. **109**, 5868 (2009)
34. E.M. Therézio, J.L. Duarte, E. Laureto, E. Di Mauro, I.L. Dias, A. Marletta, H. de Santana, J. Phys. Org. Chem. **24**, 640 (2011)
35. E.C.R. Maia, D.C. Bento, E. Laureto, D.A.M. Zaia, E.M. Therézio, G.J. Moore, H. De Santana, J. Serb. Chem. Soc. **78**, 507 (2013)
36. T.N.M. Cervantes, D.C. Bento, E.C.R. Maia, D.A.M. Zaia, E. Laureto, M.A.T. Silva, G.J. Moore, H. de Santana, J. Mater. Sci.: Mater. Electron. **23**, 1916 (2012)
37. G.A. dos Reis, I.F.L. Dias, H. de Santana, J.L. Duarte, E. Laureto, E. Di Mauro, M.A.T. da Silva, Synth. Met. **161**, 340 (2011)
38. I. Villareal, E. Morales, J.L. Acosta, Polymer **42**, 3779 (2001)
39. Y. Yagci, F. Yilmaz, S. Kiralp, L. Toppare, Macromol. Chem. Phys. **206**, 1178 (2006)
40. B. Gadgil, P. Damlin, T. Ääritalo, J. Kankare, C. Kvarnström, Electrochim. Acta **97**, 378 (2013)
41. M.R.V. Lanza, R. Bertazzoli, J. Appl. Electrochem. **30**, 61 (2000)